Ordered aeschynite-type polar magnets $RFeWO_6$ (R = Dy, Eu, Tb, and Y): A new family of type-II multiferroics

Somnath Ghara,[1] Emmanuelle Suard,[2] François Fauth,[3] T. Thao Tran,[4] P. Shiv Halasyamani,[4] Akira Iyo,[5] Juan Rodríguez-Carvajal,[2] and A. Sundaresan[1,*]

[1]*Chemistry and Physics of Materials Unit, International Centre for Materials Science, Jawaharlal Nehru Centre for Advanced Scientific Research, Jakkur P.O., Bangalore 560 064, India*

[2]*Institut Laue-Langevin, 71, Avenue des Martyrs, CS 20156, 38042 Grenoble Cedex 9, France*

[3]*CELLS-ALBA Synchrotron, BP1413, 08290 Cerdanyola del Vallès, Barcelona, Spain*

[4]*Department of Chemistry, University of Houston, 112 Fleming Building, Houston, Texas 77204, USA*

[5]*NeRI, National Institute of Advanced Industrial Science and Technology, Tsukuba, Ibaraki 305-8568, Japan*

(Received 11 April 2017; published 13 June 2017)

We report the discovery of magnetoelectric multiferroicity in a family of oxides, $RFeWO_6$ (R = Dy, Eu, Tb, and Y) that crystallize in a polar aeschynite-type structure ($Pna2_1$) with an ordered arrangement of Fe^{3+} and W^{6+} ions. Magnetization and analysis of neutron-diffraction data of $DyFeWO_6$ reveal a commensurate noncollinear antiferromagnetic ordering of Fe^{3+} spins ($T_N^{Fe} \sim 18$ K), which induce Dy spins to order at the same temperature. A sudden change in electric polarization (ΔP) appears in all the compounds at $T_N^{Fe} = 15$–18 K. The electric polarization is sensitive to an applied magnetic field, and the coupling between different magnetic R-ion and Fe-ion moments suppresses the polarization to a different extent. Although the measured polarization in polycrystalline $DyFeWO_6$ at 3.5 K is about 3 $\mu C/m^2$, a simple calculation of the ionic contribution to polarization with formal charges is 75 560 $\mu C/m^2$ and it is of the form $\mathbf{P} = (p_x, 0, p_z)$ where, p_x comes from magnetic ordering and p_z is associated with the polar structure in the paramagnetic state. These findings open up an avenue to explore further new polar magnets with rare-earth/transition-metal ions in the ordered aeschynite-type structure.

DOI: 10.1103/PhysRevB.95.224416

I. INTRODUCTION

Magnetoelectric multiferroics have been the subject of intense investigation in the past two decades because they not only offer new possibilities in device applications, but also pose a challenge in combining electric and magnetic order in the same material [1–4]. Since the mechanism of classical ferroelectrics is antagonistic with the requirement for magnetism, several new approaches have been successful in combining these two properties in the same material [1]. Perovskites are the simplest and most investigated structure type for multiferroic properties. The best example is the polar ($R3m$) magnetic compound $BiFeO_3$ which shows ferroelectric ordering at T_C = 1100 K due to polar distortion arising from the stereochemical activity of lone pair electrons of Bi^{3+} ions and magnetism from the ordering of Fe^{3+} spins (T_N = 640 K) [5,6]. Materials that belong to this class where the long-range ordering of electric dipoles and spins occur independently at two different temperatures are classified as type-I multiferroics [1]. On the other hand, the centrosymmetric ($Pnma$) perovskite $TbMnO_3$ is an example for type-II multiferroics where the ferroelectricity is induced by breaking of inversion symmetry due to magnetic ordering ($\sim$28 K) of Mn^{3+} spins [1,7]. Since the electric polarization in this class of materials is induced by spin ordering, one can control electric polarization by a magnetic field and magnetism by an electric field, which has led to tremendous interest in type-II multiferroics [4]. Most of the type-II multiferroics are centrosymmetric in the paramagnetic state.

Recently, another kind of polar magnet has been reported to exhibit magnetoelectric and/or multiferroic properties. Unlike the polar magnets that belong to type-I multiferroics where the polar distortion is caused by nonmagnetic ions, the noncentrosymmetric distortion in this kind of polar magnet is associated with magnetic atoms and thus they promise a strong magnetoelectric coupling. Thus, the polar magnets having their origin at the same source can form a subclass of type-II multiferroics. For example, the polar compounds $M_2Mo_3O_8$ (M = Fe and Mn), which crystallize in the hexagonal structure with space-group $P6_3mc$, display electric polarization below magnetic ordering temperatures [8–10]. The interesting and promising feature of these compounds is the observation of a large linear magnetoelectric effect. A similar magnetoelectric effect is observed in another polar compound $CaBaCo_4O_7$ where a nonswitchable spontaneous polarization appears below the ferrimagnetic ordering [11,12]. Collinear antiferromagnetic oxide Ni_3TeO_6 with a polar corundum structure (space-group $R3$) exhibits a nonhysteretic magnetoelectric effect [13]. Several polar corundum derivatives $A_2BB'O_6$ ($R3c$) have been reported to exhibit multiferroic properties [14–17]. Recently, a high-pressure synthesized $GaFeO_3$ with partial cation ordering in the $LiNbO_3$ structure has been shown to be magnetoelectric [18].

In this article, we report the magnetoelectric multiferroic properties of a family of polar magnets $RFeWO_6$ (R = Dy, Eu, Tb, and Y), which are derived from the centrosymmetric aeschynite structure by cation ordering. The most common representative oxide in the aeschynite structure is $CaTa_2O_6$, which has the orthorhombic structure ($Pnma$) and consists of dimers of edge-shared $Ta^{5+}O_6$ octahedra, which are connected by corner sharing to form a three-dimensional network as shown in Fig. 1(c) [19]. The compounds $RTiTaO_6$ (R = La to Dy) also crystallize in the aeschynite structure where Ti^{4+} and Ta^{5+} ions are distributed randomly in a unique crystallographic site, similar to the arrangement of $Ta^{5+}O_6$

*sundaresan@jncasr.ac.in

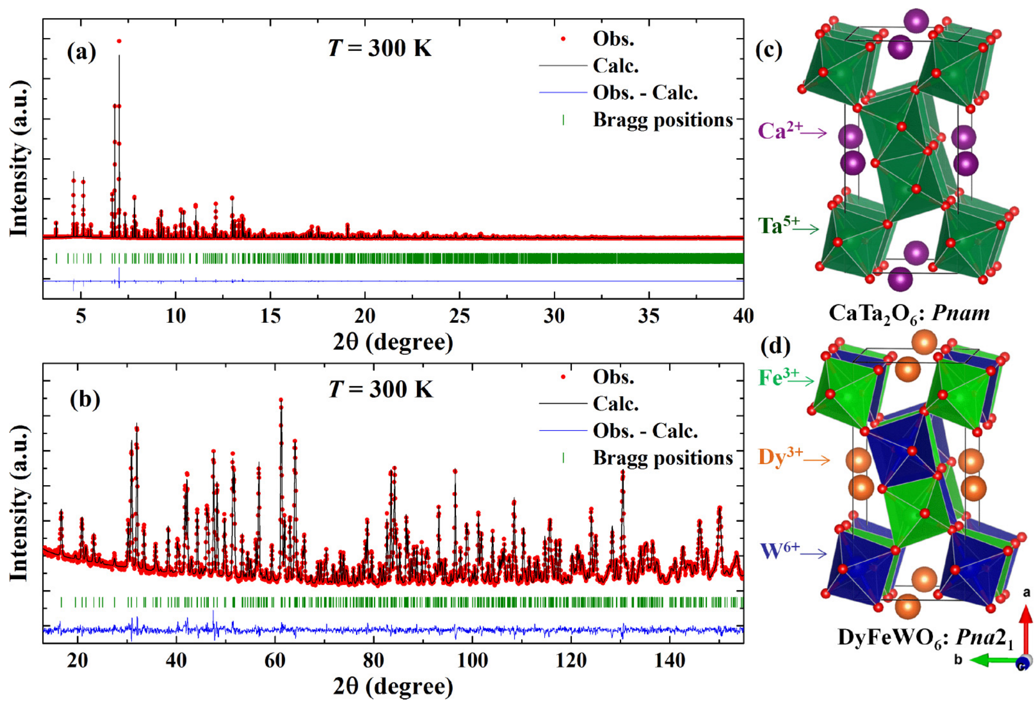

FIG. 1. Results of combined Rietveld refinement of room-temperature (a) synchrotron x-ray- and (b) neutron-diffraction data of $DyFeWO_6$. (c) The aeschynite-type crystal structure of $CaTa_2O_6$. (d) The ordered aeschynite-type crystal structure of $DyFeWO_6$.

octahedra in $CaTa_2O_6$ [20]. On the other hand, the oxides $RMWO_6$ (R = rare-earth element and M = V, Cr, Fe) have been suggested to exhibit an ordered arrangement of M^{3+} and W^{6+} ions in the aeschynite structure with the polar space-group $Pn2_1a$ [21]. However, this early report did not include any details of structural parameters and physical properties.

From a detailed structural analysis using synchrotron and neutron-diffraction data, we have confirmed that these oxides, RFeWO$_6$ with R = Dy, Eu, Tb, and Y, indeed crystallize in an ordered aeschynite-type structure with the polar $Pna2_1$ space group. Temperature-dependent dc magnetization, neutron-diffraction, and heat-capacity measurements reveal that these oxides exhibit a long-range antiferromagnetic ordering of Fe^{3+} ions at $T_N^{Fe} \sim 15$–18 K. Observation of a dielectric anomaly and an electric polarization below T_N^{Fe} and their responses under magnetic fields demonstrate that RFeWO$_6$ (R = Dy, Eu, Tb, and Y) constitute a new family of type-II multiferroics.

II. EXPERIMENTAL DETAILS

Polycrystalline samples of RFeWO$_6$, (R = Dy, Eu, and Tb) oxides were prepared by a conventional solid-state synthesis method through a two-step process. First, the compounds RFeO$_3$ (R = Dy, Eu, and Tb) were prepared by mixing a stoichiometric amount of R_2O_3 (R = Dy and Eu) or Tb_4O_7 with Fe_2O_3 and heating at the final temperature of 1350 °C for 24 h in air with several intermittent grindings. All the rare-earth oxides were preheated at 900 °C for 12 h in air before use. In the second step, RFeO$_3$ and WO_3 were mixed stoichiometrically, and the mixtures were heated at final temperatures of 1020, 1110, and 1060 °C for 12 h in a pure argon atmosphere for R = Dy, Eu, and Tb, respectively. $YFeWO_6$ was prepared at a high pressure (4.5 Gpa) and a high temperature (1000 °C) using a multianvil cubic high-pressure apparatus from the starting materials, Y_2O_3, Fe_2O_3, and WO_3.

Room-temperature synchrotron x-ray-diffraction data for all the samples were collected at the Materials Science Powder Diffraction beamline (BL04-MSPD) of the ALBA synchrotron facility at Barcelona, Spain using the wavelengths $\lambda = 0.3544$ and 0.3171 Å [22,23]. Additional data also were collected at low temperatures for $DyFeWO_6$. Neutron-diffraction data were recorded on $DyFeWO_6$ on the D2B diffractometer at the Institut Laue-Langevin (Grenoble, France) with a wavelength of $\lambda = 1.594$ Å at all temperatures. Room-temperature neutron-diffraction data on $TbFeWO_6$ also were collected with the same wavelength on the D2B diffractometer. Room-temperature powder second-harmonic generation (SHG) measurements were performed on $DyFeWO_6$ and $EuFeWO_6$ using a modified Kurtz-nonlinear optical system with a pulsed Nd:yttrium aluminum garnet laser ($\lambda = 1064$ nm). The details of equipment and methodology have already been reported [24–26].

dc magnetization measurements were carried out with a superconducting quantum interference device (Quantum Design, USA). Temperature-dependent magnetization was measured under a field-cooled (FC) condition where the sample was cooled under a magnetic field of 100 Oe and the data were recorded during heating with a rate of 3 K/min. Magnetic-field-dependent magnetization measurements at fixed temperatures were carried out with stability at each field mode. Heat capacity was measured in a physical property measurement system [(PPMS) Quantum Design] using a relaxation technique. A temperature-dependent dielectric constant was measured under different frequencies and various applied magnetic fields with an Agilent E4980A LCR meter with a rate of 2 K/min. The pyroelectric current was measured with

TABLE I. Structural parameters obtained from a combined Rietveld refinement of room-temperature synchrotron x-ray- ($\lambda = 0.3544$ Å) and neutron- ($\lambda = 1.594$ Å) diffraction data of $DyFeWO_6$.

Atom	Wyckoff position	x	y	z	B_{iso} (Å^2)	Occupancy
Dy	4*a*	0.0426(1)	0.4570(2)	0.25	0.49(1)	1
Fe	4*a*	0.1378(2)	0.9661(5)	0.9925(5)	0.80(4)	1
W	4*a*	0.3539(1)	0.4519(2)	0.0057(3)	0.13(1)	1
O1	4*a*	0.9703(7)	0.7683(15)	0.0424(14)	0.77(17)	1
O2	4*a*	0.5221(7)	0.2542(16)	0.9610(15)	0.99(19)	1
O3	4*a*	0.2130 (8)	0.6145(19)	0.0622 (15)	1.24(19)	1
O4	4*a*	0.2919(8)	0.1278(17)	0.9333(13)	0.68(16)	1
O5	4*a*	0.1437(3)	0.0590(7)	0.2583(16)	0.94(6)	1
O6	4*a*	0.1197(3)	0.8289(6)	0.7500 (20)	0.83(6)	1

Space group: $Pna2_1$; Cell dimension: $a = 10.97992(2)$ Å, $b = 5.18849(1)$ Å, $c = 7.34824(1)$ Å, $\alpha = \beta = \gamma = 90^\circ$, $V = 418.624(1)$ Å^3; Goodness of fit: $\chi^2 = 1.75$, Reliability factors: $R_{\mathrm{Bragg}}(\%) = 3.66$, $R_f(\%) = 2.36$ (for the neutron data); $\chi^2 = 1.07$, $R_{\mathrm{Bragg}}(\%) = 3.67$, $R_f(\%) = 2.80$ (for synchrotron data).

a Keithley 6517A electrometer. In the pyroelectric current measurements, the sample was cooled across the magnetic ordering temperature with an electric field and then shorted for 45 min to remove stray charges, and then the current was recorded during heating with a rate of 10 K/min. A PPMS was used for temperature- and magnetic-field-dependent dielectric and pyroelectric current measurements with the help of a multifunctional probe provided by Quantum Design. For dc-biased current measurements, the sample was cooled to the lowest temperature without any poling field. At the lowest temperatures, the dc electric field was applied, and the current was recorded while warming the sample with a rate of 10 K/min under the electric field [27]. For all electrical measurements, contacts were made on sintered pellet samples with a high performance silver paste from Ted Pella, Inc.

III. RESULTS AND DISCUSSION

In this section, first we present a detailed analysis of the crystal and magnetic structures and the results of multiferroicity in $DyFeWO_6$. Then, we discuss the experimental results in other oxides $RFeWO_6$ (R = Eu, Tb, and Y).

A. $DyFeWO_6$

To determine the crystal structure at room temperature, the synchrotron powder x-ray-diffraction pattern of $DyFeWO_6$ was indexed with the DICVOL program available in the FULLPROF suite [28]. The reflection conditions obtained from indexing are as follows: $0kl : k + l = 2n, hk0 : h = 2n$, which suggest that the most probable space groups could be either $Pnma$ or $Pn2_1a$. Since the reflection condition for both of these space groups is the same, it is not possible to conclude the real space group at this stage of analysis using diffraction data. However, $Pnma$ is centrosymmetric, whereas $Pn2_1a$ is a polar space group. SHG measurements revealed that this material is SHG active with an efficiency comparable to that of α-SiO_2 supporting the polar space-group $Pn2_1a$. Therefore, to determine the complete structure, we have performed a combined Rietveld refinement analysis of the room-temperature synchrotron x-ray- and neutron-diffraction data using the FULLPROF software. In this process, we have used the standard setting of $Pna2_1$ (space-group No. 33) instead of the nonstandard $Pn2_1a$ setting. Since the atomic positions are not known and $Pna2_1$ is a subgroup of $Pnam$ (another setting of $Pnma$), the atomic positions in $CaTa_2O_6$ in the $Pnma$ space group have been used and converted to the $Pna2_1$ space group using the SUBGROUPGRAPH and TRANSTRU programs available on the Bilbao crystallographic server [29]. The refined synchrotron x-ray and neutron-diffraction patterns are shown in Figs. 1(a) and 1(b), respectively, and the obtained crystal structure of $DyFeWO_6$ is displayed in Fig. 1(d). The detailed structural parameters obtained from the refinements are given in Table I. It is observed that the 8*d* octahedral site in the centrosymmetric *Pnam* structure [Fig. 1(c)] of $CaTa_2O_6$ splits into two 4*a* octahedral sites in $Pna2_1$ where Fe^{3+} and W^{6+} ions are arranged in an ordered manner. The cation ordering occurs because of the size and charge differences between Fe^{3+} and W^{6+} ions. $Fe^{3+}O_6$ and $W^{6+}O_6$ octahedra form edge-shared dimers which are connected through corner sharing to form a three-dimensional structure. The selected bond lengths obtained from refinement are shown in Table II. The average ⟨Dy-O⟩, ⟨Fe-O⟩, and ⟨W-O⟩ bond lengths, 2.38, 2.00, and 1.94 Å, respectively, are consistent with those reported in $DyFeO_3$ and $MnWO_4$, indicating Dy^{3+}, Fe^{3+}, and W^{6+} oxidation states [30,31]. Furthermore, the results of the bond valence sum calculations as shown in Table II, confirm the +3 and +6 oxidation states of Dy/Fe and W ions, respectively.

Figure 2(a) shows temperature dependence of magnetization data $M(T)$ measured with an applied field of 100 Oe

TABLE II. Selected bond lengths (Å) and bond valence sum (BVS) for $DyFeWO_6$ at room-temperature.

Cation	O1	O2	O3	O4	O5	O6
	2.36(1)	2.30(1)				
Dy			2.46(1)	2.43(1)	2.34(0)	2.32(0)
	2.45(1)	2.40(1)				
Fe	2.14(1)	1.94(1)	2.07(1)	1.94(1)	2.01(1)	1.93(1)
W	1.95(1)	2.14(1)	1.81(1)	1.89(1)	1.90 (1)	1.93(1)
	BVS Dy			2.88(2)		
	BVS Fe			3.15(4)		
	BVS W			5.88(7)		

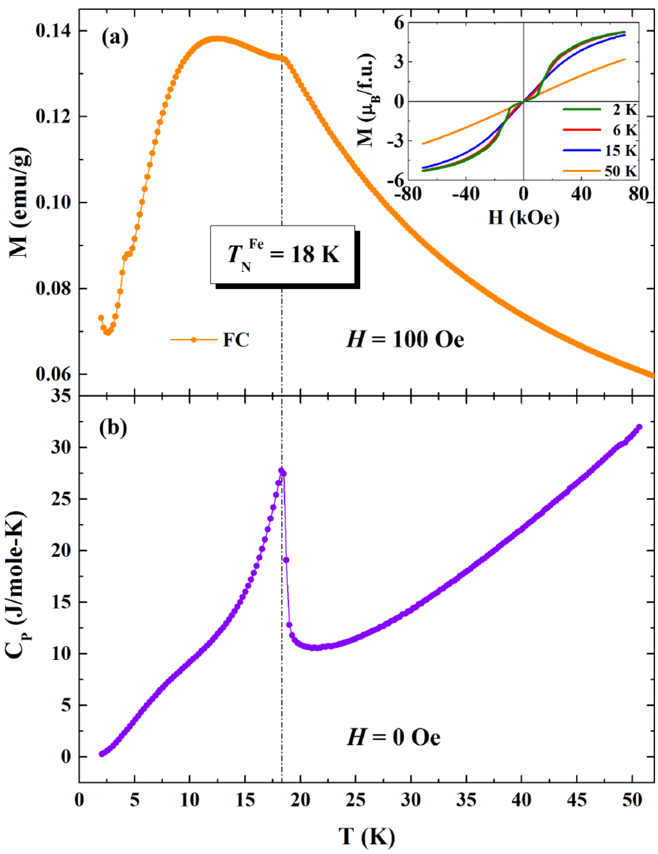

FIG. 2. (a) Temperature dependence of field-cooled magnetization of $DyFeWO_6$ under a magnetic field of 100 Oe. The inset shows magnetic-field-dependent magnetization at different temperatures. (b) Temperature-dependent heat capacity (C_P) of $DyFeWO_6$.

under the FC condition. A clear humplike anomaly in $M(T)$ and the sharp λ anomaly in the heat-capacity $C_P(T)$ at 18 K as seen in Fig. 2(b) indicate the long-range antiferromagnetic ordering of Fe^{3+} spins. Upon further cooling, $M(T)$ increases and exhibits a broad maximum around 12 K. At 5 K, there is a step in the $M(T)$ data indicating a long-range cooperative antiferromagnetic ordering of Dy^{3+} moments. Indeed, as discussed later, our neutron-diffraction results reveal that the Fe^{3+} ordered moments induce Dy^{3+} moments to order with the same propagation vector at 18 K. Because of this, we do not find any anomaly in $C_P(T)$ at the independent ordering temperature (5 K) of the Dy^{3+} moments. Temperature-dependent inverse susceptibility ($1/\chi_{mol}$) data could be fitted with the Curie-Weiss law at higher temperatures (not shown). The obtained effective paramagnetic moment (μ_{eff}) is 12.5 μ_B/f.u. (where f.u. represents formula unit), which is close to the theoretical moment (12.17 μ_B/f.u.) for Dy^{3+} and Fe^{3+} moments. The Curie-Weiss temperature (θ_{CW}) obtained from the fit is −21 K. This is consistent with the observed antiferromagnetic ordering at 18 K. The magnetic-field-dependent magnetizations $M(H)$ at different temperatures are shown in the inset of Fig. 2(a). The $M(H)$ curve at 15 K is consistent with the antiferromagnetic behavior. However, at 2 K, the $M(H)$ data exhibit field-induced steps indicating the metamagnetic nature of Dy^{3+} magnetism. Above 18 K, the $M(H)$ curve resembles paramagnetic behavior.

In order to understand the magnetization behavior and determine the magnetic structure, low-temperature neutron-diffraction data have been analyzed. In Fig. 3(a), the neutron-diffraction pattern recorded at 3.5 K is shown where Rietveld refinement has been performed including the magnetic and nuclear structure models. The magnetic structure has been solved using symmetry analysis with both BASIREPS (FULLPROF suite) and MAXMAGN (the Bilbao crystallographic server) programs [32]. BASIREPS provides a complex two-dimensional irreducible representation that is transformed to real using physically irreducible representations from the table of Campbell *et al.* [33]. The 12 basis functions obtained indicate that we have to impose special directions in the representation space (put constraints on the coefficients) in order to get more symmetric magnetic structures, otherwise we obtain triclinic structures. Using MAXMAGN, we obtain three maximal magnetic space groups compatible with the propagation vector $\mathbf{k} = (0,1/2,1/2)$, these are as follows: C_ac, P_ac, and P_S1. The magnetic space-group C_ac describes correctly the diffraction pattern and corresponds to a particular selection of basis vectors obtained with BASIREPS. Using the Belov-Neronova-Smirnova (BNS) notation, the transformation from the setting we use, related to the paramagnetic basis as $(a,2b,2c;0,0,0)$ to the standard BNS cell is $(-c,b,a;0,1/8,0)$, so the b axis is kept and the glide plane c of C_ac is the original glide plane a perpendicular to the b axis of $Pna2_1$ [34]. We have used the formalism of propagation vectors by using the crystallographic unit cell as the basis for describing the magnetic structure and replacing the antitranslations and centering translations of the magnetic structure when described in the magnetic unit cell by the effect of the propagation vector. The small metric distortion due to the reduction of symmetry to monoclinic cannot be detected with the resolution of the present neutron and synchrotron measurements. Only an anomaly in the evolution of the cell parameters as a function of temperature can clearly be seen at T_N^{Fe} in the synchrotron data (not shown). However, very small changes in the intensities of Bragg reflection may contain information about the distortion of the crystal structure. We have used a recently implemented option in FULLPROF that allows for combining crystallographic and magnetic symmetry modes in order to determine the structural changes accompanying the magnetic ordering (discussed later). From the point of view of symmetry, the magnetic point group derived from C_ac is $m1'$ with m perpendicular to the b axis of the paramagnetic space group, and therefore the macroscopic properties in the magnetically ordered phase are driven by this group. The allowed electric polarization is constrained to be within the m plane so that in the magnetic phase the polarization should be of the form $\mathbf{P}_m = (p_x,0,p_z)$. The paramagnetic group $Pna2_11'$ is already polar, and the allowed polarization, even if it is not detected experimentally, is of the form $\mathbf{P} = (0,0,p_z)$, so in the magnetic phase a new component is allowed.

We observe a very unusual behavior of Dy^{3+} magnetism in this compound. If we do not consider the Dy^{3+} moment in refining neutron diffraction data recorded at 15 K, we could refine the pattern, but the magnetic moment of Fe^{3+} becomes 5.7 μ_B which is too high. This implies that there should be a contribution of Dy^{3+} moments at 15 K probably induced by the ordering of Fe spins. In order to confirm this, we refined

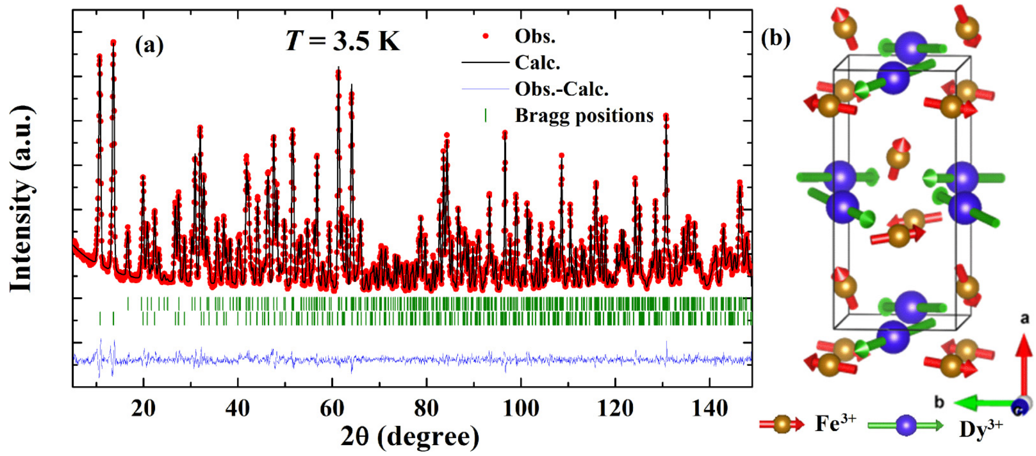

FIG. 3. (a) Results of Rietveld refinement of neutron-diffraction data of $DyFeWO_6$ collected at 3.5 K. The first row of vertical bars represents the nuclear Bragg positions, and the second row represents magnetic Bragg peak positions. (b) The magnetic structure of $DyFeWO_6$.

the neutron data at 15, 10, and 3.5 K, including the magnetic contribution of Dy with the same propagation vector of Fe spins. This model gave a best fit to the data with good reliability parameters, and the obtained magnetic moments of Fe^{3+} and Dy^{3+} ions are given in Table III where the crystallographic parameters at 3.5 K also are shown.

The obtained magnetic structure at 3.5 K is shown in Fig. 3(b). It is interesting to note the unusual arrangement of both Fe and Dy spins in this compound. There are two different Fe spin sites. In each site, the spins are aligned antiferromagnetically, but between the sites (along the *a* axis) they are nearly perpendicular to each other and thus the structure is strongly noncollinear. A similar noncollinear arrangement of Dy spins is observed with a tendency to get nearly perpendicular Dy^{3+} moments at low temperatures. This could be due to the single-ion anisotropy of Dy^{3+} ions. We found that the magnetic structure remains the same in the temperature range between 3.5 and 18 K despite the independent magnetic correlations developing among Dy^{3+} spins below 5 K. The magnetic structure is essentially noncentrosymmetric as the underlying crystal structure is polar. This kind of magnetic structure is very unusual, and a model to explain the observed spin configuration still needs to be elaborated, and the detailed description of the observed magnetic structure will be published elsewhere.

Temperature dependence of the real part of dielectric constant $\varepsilon'(T)$ measured with different frequencies is shown in Fig. 4(a). A clear peak is observed around the magnetic ordering temperature of $T_N^{Fe} = 18$ K in $\varepsilon'(T)$, which is associated with a peak in the imaginary part of dielectric constant $\varepsilon''(T)$ [shown in the inset of Fig. 4(a)]. These peaks in $\varepsilon'(T)$ and $\varepsilon''(T)$ around T_N^{Fe} do not shift with increasing frequency, which indicates that these are not associated with any relaxation phenomenon. However, another broad peak is found in $\varepsilon''(T)$ at further lower temperatures, which shifts to higher temperatures with increasing frequency, indicating that it is associated with the intrinsic dielectric relaxation of the material. Note that the value of dielectric loss ($\tan\delta = \frac{\varepsilon''}{\varepsilon'}$) is very small ($\sim$0.02) at

TABLE III. Crystallographic parameters of $DyFeWO_6$ at 3.5 K obtained from Rietveld refinement of neutron-diffraction data. Ordered magnetic moments at different temperatures are shown in the bottom rows.

Name	Wyckoff position	x	y	z	B_{iso} (Å^2)	Occupancy
Dy	4a	0.0424(1)	0.4576(2)	0.25	0.43(2)	1
Fe	4a	0.1363(4)	0.9642(10)	0.9936(10)	0.86(9)	1
W	4a	0.3530(6)	0.4572(16)	0.0095(15)	0.07(13)	1
O1	4a	0.9732(7)	0.7639(15)	0.0385(17)	0.23(14)	1
O2	4a	0.5234(10)	0.2579(20)	0.9550(22)	1.48(22)	1
O3	4a	0.2151(8)	0.6088(19)	0.0630(14)	1.47(20)	1
O4	4a	0.2938(6)	0.1290(13)	0.9342(11)	0.11(13)	1
O5	4a	0.1437(3)	0.0593(7)	0.2522(24)	0.83(5)	1
O6	4a	0.1204(3)	0.8290(6)	0.7466(20)	0.56(6)	1

Ordered magnetic moments

T (K)	$\mu_{Dy^{3+}}$ (μ_B)	$\mu_{Fe^{3+}}$ (μ_B)
3.5	7.90(4)	4.48(9)
10	5.71(6)	4.29(12)
15	3.57(9)	3.87(17)

Cell dimension: $a = 10.97334(11)$ Å, $b = 5.18423(5)$ Å, $c = 7.33767(7)$ Å, $\alpha = \beta = \gamma = 90^\circ$, $V = 417.427(7)$ Å^3, Goodness of fit: $\chi^2 = 2.25$; Reliability factors: $R_{Bragg}(\%) = 2.22$, $R_f(\%) = 1.22$.

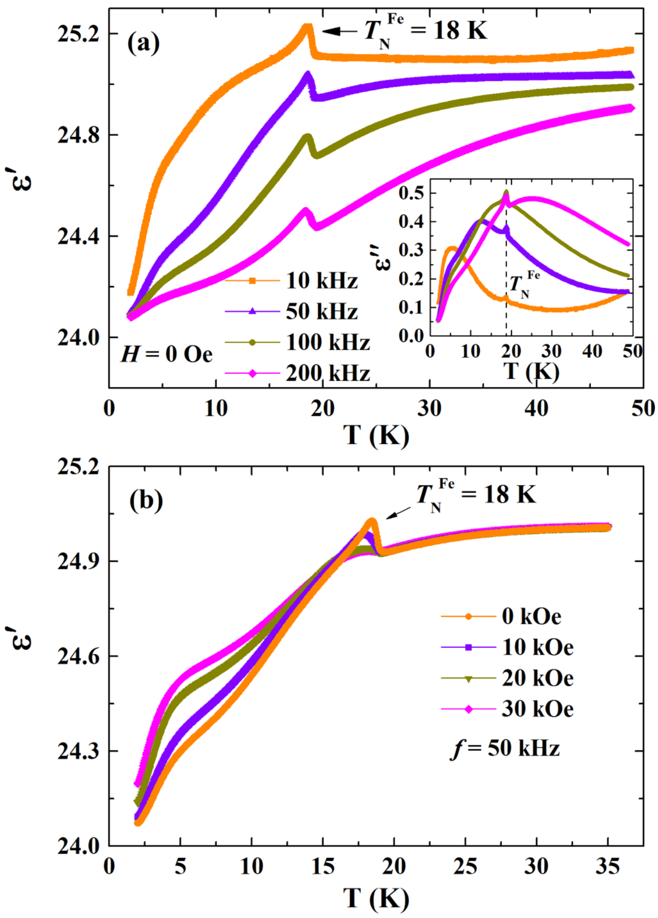

FIG. 4. (a) Temperature variation of the real part of dielectric constant $\varepsilon'(T)$ of $DyFeWO_6$ measured with different frequencies. The inset shows the corresponding imaginary part of the dielectric constant $\varepsilon''(T)$. (b) Temperature dependence of the real part of dielectric constant $\varepsilon'(T)$ at 50 kHz measured in the presence of different applied magnetic fields.

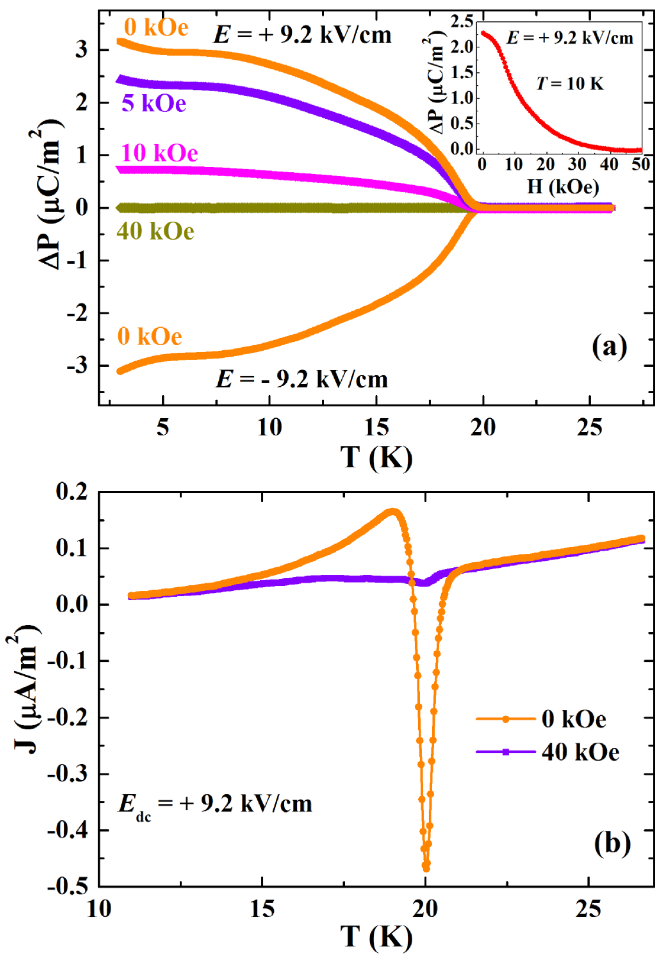

FIG. 5. (a) Temperature evolution of electric polarization $\Delta P(T)$ of $DyFeWO_6$ below $T_N^{Fe} = 18$ K obtained from pyroelectric current measurements under an electric field of $E = \pm 9.2$ kV/cm and different magnetic fields. The inset shows a magnetic-field-dependent change in electric polarization measured at 10 K with a ramping magnetic field with a rate of 120 Oe/s after poling the sample with an electric field of $E = +9.2$ kV/cm. (b) Temperature dependence of a dc-biased current of $DyFeWO_6$ measured with an electric field of $E_{dc} = +9.2$ kV/cm and magnetic fields of 0 and 40 kOe.

50 kHz around T_N^{Fe}, which suggests that the compound is highly insulating at low temperatures. Thus, the occurrence of a dielectric anomaly at the magnetic ordering temperature indicates a close correlation between magnetic and dielectric properties. This correlation is further confirmed from a temperature-dependent dielectric constant measured with 50 kHz under different magnetic fields [Fig. 4(b)]. The magnetic field strongly suppresses the anomaly around T_N^{Fe} in $\varepsilon'(T)$. At further lower temperatures, $\varepsilon'(T)$ increases with an increasing magnetic field, indicating a possible field-induced change in the magnetic structure of Dy^{3+} spins. Thus, Figs. 4(a) and 4(b) confirm that a strong magnetodielectric effect is present below T_N^{Fe} in the present system.

To investigate whether the dielectric anomaly is associated with the appearance of electric polarization, a pyroelectric current was measured with an applied electric field of $E = \pm 9.2$ kV/cm and different applied magnetic fields. The electric polarization $\Delta P(T)$ obtained by integrating the pyroelectric current with measurement duration is displayed in Fig. 5(a). The presence of a sharp asymmetric pyroelectric current peak at zero magnetic field indicates the appearance of electric polarization below T_N^{Fe}. Since this compound has a polar structure, there can be a nonzero electric polarization (p_z) above T_N^{Fe}. However, we could not find measurable polarization in the paramagnetic region, indicating that this compound is only pyroelectric or the switchable polarization is too small to be measured. The observed electric polarization below T_N^{Fe} is the result of the possible enhancement of the high-temperature electric polarization (p_z) and the emergence of the new component p_x due to magnetic ordering of Fe^{3+} ions as discussed above. It can be seen from Fig. 5(a) that the electric polarization also is affected by the external magnetic field as observed in $\varepsilon'(T)$ in Fig. 4(b) and vanished under a magnetic field of 40 kOe. In the inset of Fig. 5(a), magnetic-field-dependent electric polarization measured at 10 K is shown, and it clearly demonstrates the suppression of electric polarization under an applied magnetic field. Thus, the presence of the dielectric anomaly and electric polarization below T_N^{Fe} and their responses under the magnetic field suggest that the present compound is a magnetoelectric multiferroic or type-II multiferroic. However the magnetic point group $m1'$ forbids the first-order magnetoelectric effect, so only the second-order inverse magnetoelectric tensor ($P_i = \alpha_{ijk}^T H_j H_k$) is allowed. Although the pyroelectric current can be switched in the polycrystalline sample by applying an opposite poling electric field [Fig. 5(a)], it requires a single-crystal study to confirm the polarization switching.

In order to confirm that the observed pyroelectric current peak near T_N^{Fe} is due to the depolarization current associated with electric dipoles and not due to thermally stimulated free charge carriers, we measured the dc-biased current which can distinguish these two different origins as reported, where the current was recorded with increasing temperature in the presence of an applied dc electric field without any prepoling [27]. In Fig. 5(b), the temperature-dependent dc-biased current measured under an applied electric field of $E_{dc} = +9.2\,\mathrm{kV/cm}$ is shown. The dc-biased current exhibits a broad upward and then a sharp downward peak with increasing temperature. The upward broad peak is associated with the polarization of the material which slowly increases with increasing temperature in the presence of an electric field. The downward peak around T_N^{Fe} indicates the depolarization of the polarized dipoles. A small positive shift could be due to a higher warming rate (10 K/min), which is an important parameter in this measurement. These results confirm the intrinsic nature of the electric polarization. Furthermore, the absence of any feature associated with dc-biased current measured with a magnetic field of 40 kOe [Fig. 5(b)] supports the suppression of electric polarization by a magnetic field.

Using the approach of symmetry modes, we have refined the most relevant structural mode amplitudes in order to determine the most important structural change accompanying the magnetic ordering [33]. There are two active representations of the paramagnetic group $Pna2_11'$ for structural distortions GM1 and GM4, and the global refined amplitudes for both representations are as follows: A_GM1 = 0.04(1) and A_GM4 = 0.17(8) Å, the most important displacements correspond to the parents O3, O4, and O6 (which are split into two independent atoms each) with approximate displacements of 0.035 Å/atom with respect to the paramagnetic phase.

A calculation of the ionic polarization in the paramagnetic polar phase at 30 K gives a value of $6300\,\mu\mathrm{C/m^2}$ along the c axis, which arises due to a shift of the barycenter of the positive and negative charges by 0.0034 Å [35]. Although this value of polarization is measurable experimentally, we could not find any polarization because of the fact that there is no polar-nonpolar phase transition in the accessible temperature range and the polycrystalline nature of the sample. On the contrary, the same calculation in the magnetic state (3.5 K) using the resulting crystal structure from the refinement of the symmetry-mode amplitudes gives a value of an order of magnitude greater: $75560\,\mu\mathrm{C/m^2}$ (to be compared with $260000\,\mu\mathrm{C/m^2}$ for tetragonal $BaTiO_3$ [36]) with $P \approx (-62200,0,42900)\,\mu\mathrm{C/m^2}$. However, the low value of polarization obtained from pyroelectric current measurements could be due to the polycrystalline nature of the sample.

B. $EuFeWO_6$

The ordered aeschynite-type polar crystal structure (space-group $Pna2_1$) of $EuFeWO_6$ is confirmed by the Rietveld refinement of room-temperature synchrotron x-ray-diffraction data (shown in Fig. S1 of the Supplemental Material) and room-temperature SHG measurement [37]. The structural parameters obtained from refinement are given in Table S1 of the Supplemental Material [37]. In Fig. 6(a), the temperature-dependent magnetization $M(T)$ shows a peak around 17 K indicating the magnetic ordering of Fe^{3+} ions. The long-range magnetic ordering is confirmed by a sharp λ-type anomaly in $C_P(T)$ as shown in Fig. 6(b). The $M(H)$ loop at 2 K is consistent with antiferromagnetic ordering [see the inset of Fig. 6(a)]. The Curie-Weiss fit to susceptibility data at high temperatures suggests that Eu^{3+} contributes to the effective paramagnetic moment but it does not order down to 2 K as suggested by $M(T)$ and $C_P(T)$. The paramagnetic nature of Eu^{3+} moments is consistent with the increase in $M(T)$ at low temperatures. A sharp dielectric anomaly is observed around T_N^{Fe} [Fig. 6(c)], which seems to be smeared out under the magnetic field. Electric polarization is observed below T_N^{Fe} in a zero magnetic field as shown in Fig. 6(d), and it is suppressed with an increasing magnetic field. These results suggest that $EuFeWO_6$ is also a type-II multiferroic. Unlike $DyFeWO_6$, the electric polarization in $EuFeWO_6$ is suppressed at a relatively large magnetic field (80 kOe).

C. $TbFeWO_6$

Results of combined Rietveld refinement of room-temperature synchrotron x-ray- and neutron-diffraction data of $TbFeWO_6$ are shown in Fig. S2 of the Supplemental Material, and the structural parameters are given in Table S2 [37]. Temperature-dependent FC magnetization $M(T)$ measured under a magnetic field of 100 Oe is shown in Fig. 7(a) where a sharp peak is observed at 2.4 K. Heat-capacity data $C_P(T)$ exhibit two sharp λ-kind anomalies around 15 and 2.4 K [(Fig. 7(b)], suggesting long-range antiferromagnetic ordering of Fe^{3+} and Tb^{3+} spins, respectively. Because of the relatively large paramagnetic moment of Tb^{3+} ions, there is no anomaly in $M(T)$ around the Fe-ordering temperature ($T_N^{Fe} \sim 15\,\mathrm{K}$). Unlike $DyFeWO_6$ where the Dy moments are induced to order at T_N^{Fe}, the observation of the anomaly in $C_P(T)$ at $T_N^{Tb} \sim 2.4\,\mathrm{K}$ suggests that Tb^{3+} moments remain paramagnetic above $T_N^{Tb} \sim 2.4\,\mathrm{K}$. However, low-temperature neutron-diffraction measurements are required to confirm this suggestion. Magnetic-field-dependent magnetization $M(H)$ data [see the inset of Fig. 7(a)] suggest antiferromagnetic behavior below $T_N^{Fe} \sim 15\,\mathrm{K}$ and a metamagnetic behavior at 2 K due to field-induced changes associated with Tb^{3+} ordering. In Fig. 7(c), the temperature-dependent real parts of dielectric constant $\varepsilon'(T)$ measured with 50 kHz under different magnetic fields are shown. In a zero magnetic field, two sharp dielectric anomalies are observed around $T_N^{Fe} \sim 15$ and $T_N^{Tb} \sim 2.4\,\mathrm{K}$. The anomaly around T_N^{Fe} is suppressed and becomes broad under a high magnetic field, whereas the anomaly around T_N^{Tb} vanished in a high magnetic field. Temperature dependence of electric polarization $\Delta P(T)$ is shown in Fig. 7(d) where the appearance of nonzero electric polarization below $T_N^{Fe} \sim 15\,\mathrm{K}$ without an applied magnetic

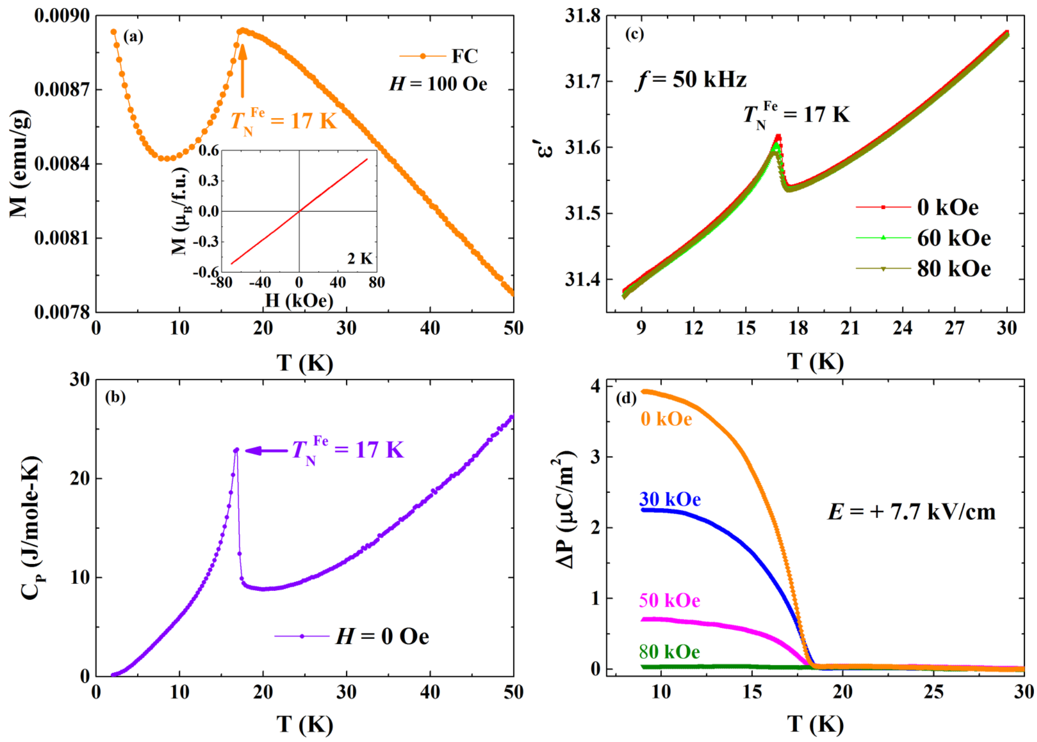

FIG. 6. (a) Variation of FC magnetization with temperature $M(T)$ under a magnetic field of 100 Oe in $EuFeWO_6$. The inset shows magnetization vs magnetic-field data measured at 2 K. (b) Temperature-dependent heat capacity (C_P) of $EuFeWO_6$. (c) Temperature variation of the real part of dielectric constant $\varepsilon'(T)$ of $EuFeWO_6$ measured with 50 kHz under different magnetic fields. (d) Evolution of electric polarization $\Delta P(T)$ with temperature below T_N^{Fe} in $EuFeWO_6$ obtained from pyroelectric current measurements with an electric field of $E = +7.7$ kV/cm and different magnetic fields.

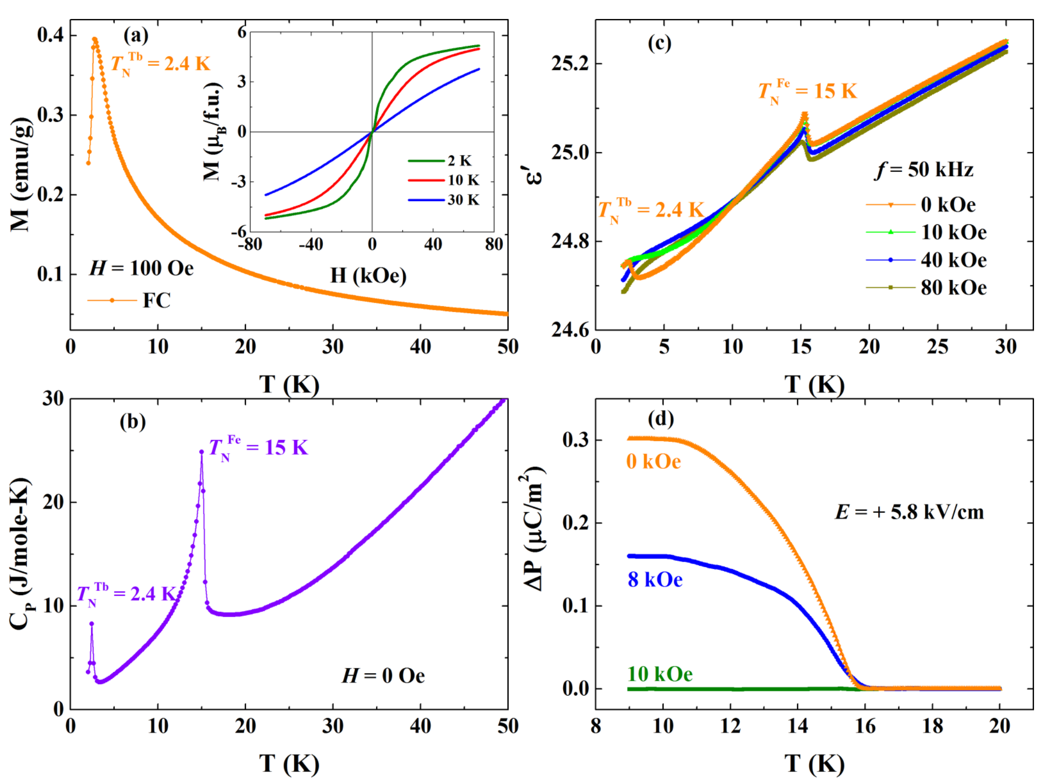

FIG. 7. (a) Temperature-dependent FC magnetization $M(T)$ of $TbFeWO_6$ measured under a magnetic field of 100 Oe. The inset shows the magnetic-field dependence of magnetization measured at different temperatures. (b) Temperature variation of heat-capacity $C_P(T)$ of $TbFeWO_6$. (c) Temperature dependence of the real part of the dielectric constant $\varepsilon'(T)$ measured with 50 kHz under different magnetic fields. (d) Electric polarization $\Delta P(T)$ measured with an electric field of $E = +5.8$ kV/cm and different applied magnetic fields.

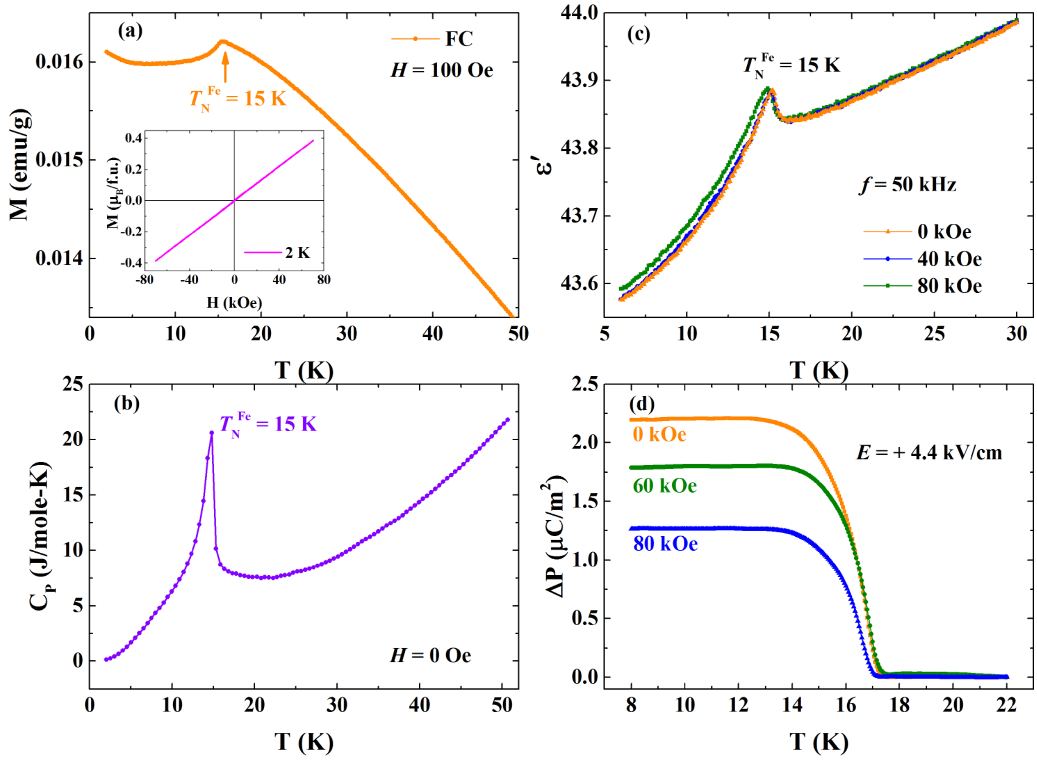

FIG. 8. (a) Temperature variation of magnetization of $YFeWO_6$ measured with a magnetic field of 100 Oe under a field-cooled condition. The $M(H)$ loop measured at 2 K is shown in the inset. (b) Temperature dependence of $C_P(T)$. (c) and (d) Temperature evolution of dielectric constant $\varepsilon'(T)$ and electric polarization $\Delta P(T)$ measured with different magnetic fields in $YFeWO_6$.

field, suggests the presence of multiferroicity in $TbFeWO_6$. The electric polarization vanishes under an applied magnetic field of 10 kOe, which indicates that a strong magnetoelectric effect is present below $T_N^{Fe} \sim 15$ K.

D. $YFeWO_6$

The synchrotron x-ray-diffraction pattern of $YFeWO_6$ and the structural parameters obtained at the final Rietveld refinement are given in Fig. S3 and Table S3, respectively, of the Supplemental Material [37]. $M(T)$ and $C_P(T)$ data are shown in Figs. 8(a) and 8(b), respectively, and the $M(H)$ data are given in the inset of Fig. 8(a). A peak observed around 15 K in both the $M(T)$ and the $C_P(T)$ data and the linear behavior of the $M(H)$ loop at 2 K suggest antiferromagnetic ordering of Fe^{3+} moments around $T_N^{Fe} \sim 15$ K. In the $\varepsilon'(T)$ data [Fig. 8(c)], a sharp anomaly is observed in the zero magnetic field around T_N^{Fe} , and it is not affected under applied magnetic fields but shifts slightly to a lower temperature at 80 kOe. $\Delta P(T)$ data measured with different magnetic fields are shown in Fig. 8(d). Similar to other compounds, electric polarization appears below T_N^{Fe}, and its magnitude decreases with applied magnetic fields. However, unlike the magnetic R ions, the electric polarization in $YFeWO_6$ does not vanish even at 80 kOe. The fact that the observation of electric polarization below $T_N^{Fe} \sim 15$ K in $YFeWO_6$ indicates that the emergence of electric polarization in $RFeWO_6$ is solely due to the long-range magnetic ordering of Fe^{3+} moments. The R-ion moments only affect the polarization through the coupling between R and Fe spins. It should be mentioned here that all these samples exhibit switchable electric polarization under a negative electric field. Although we have not determined the magnetic structure in compounds other than $DyFeWO_6$, the appearance of electric polarization at T_N^{Fe} indicates that all the compounds should have a similar magnetic structure of Fe spins.

IV. CONCLUSION

In conclusion, we have demonstrated magnetoelectric multiferroic properties in a family of oxides $RFeWO_6$ (R = Dy, Eu, Tb, and Y) which belong to a polar aeschynite-type structure. A new kind of unusual commensurate and noncollinear magnetic structure of Fe^{3+} spins is responsible for enhancing the electric polarization below the magnetic ordering temperature. The magnetic coupling between R and Fe ions has a strong effect on the electric polarization. It requires further studies to understand the mechanism of polarization associated with magnetic ordering and the effect of coupling between R and Fe spins on the electric polarization. Finding magnetoelectric properties in this class of compounds opens up an avenue for exploring new polar magnets with high magnetic ordering temperature.

ACKNOWLEDGMENTS

A.S. and S.G. thank the Department of Science and Technology, India (Grant No. SR/NM/Z-07/2015) for financial support for performing synchrotron x-ray-diffraction experiments at ALBA, Barcelona, Spain and Jawaharlal Nehru

Centre for Advanced Scientific Research for managing the project. A.S. and S.G. acknowledge Sheikh Saqr Laboratory at Jawaharlal Nehru Centre for Advanced Scientific Research for providing experimental facilities. S.G. acknowledges Jawaharlal Nehru Centre for Advanced Scientific Research for providing a research fellowship (JNC/S0349). P.S.H. and T.T.T. thank the Welch Foundation (Grant No. E-1457) and Grant No. NSF-DMR-1503573 for support.

[1] D. Khomskii, Trend: Classifying multiferroics: Mechanisms and effects, Physics **2**, 20 (2009).

[2] W. Eerenstein, N. Mathur, and J. F. Scott, Multiferroic and magnetoelectric materials, Nature (London) **442**, 759 (2006).

[3] S.-W. Cheong and M. Mostovoy, Multiferroics: A magnetic twist for ferroelectricity, Nature Mater. **6**, 13 (2007).

[4] Y. Tokura, S. Seki, and N. Nagaosa, Multiferroics of spin origin, Rep. Prog. Phys. **77**, 076501 (2014).

[5] G. Smolenskiĭ and I. Chupis, Ferroelectromagnets, Soviet Phys.-Usp. **25**, 475 (1982).

[6] J. Wang, J. Neaton, H. Zheng, V. Nagarajan, S. Ogale, B. Liu, D. Viehland, V. Vaithyanathan, D. Schlom, and U. Waghmare, Epitaxial $BiFeO_3$ multiferroic thin film heterostructures, Science **299**, 1719 (2003).

[7] T. Kimura, T. Goto, H. Shintani, K. Ishizaka, T. Arima, and Y. Tokura, Magnetic control of ferroelectric polarization, Nature (London) **426**, 55 (2003).

[8] Y. Wang, G. L. Pascut, B. Gao, T. A. Tyson, K. Haule, V. Kiryukhin, and S.-W. Cheong, Unveiling hidden ferrimagnetism and giant magnetoelectricity in polar magnet $Fe_2Mo_3O_8$, Sci. Rep. **5**, 12268 (2015).

[9] T. Kurumaji, S. Ishiwata, and Y. Tokura, Doping-Tunable Ferrimagnetic Phase with Large Linear Magnetoelectric Effect in a Polar Magnet $Fe_2Mo_3O_8$, Phys. Rev. X **5**, 031034 (2015).

[10] T. Kurumaji, S. Ishiwata, and Y. Tokura, Diagonal magnetoelectric susceptibility and effect of Fe doping in the polar ferrimagnet $Mn_2Mo_3O_8$, Phys. Rev. B **95**, 045142 (2017).

[11] V. Caignaert, A. Maignan, K. Singh, C. Simon, V. Pralong, B. Raveau, J. F. Mitchell, H. Zheng, A. Huq, and L. Chapon, Gigantic magnetic-field-induced polarization and magnetoelectric coupling in a ferrimagnetic oxide $CaBaCo_4O_7$, Phys. Rev. B **88**, 174403 (2013).

[12] R. Johnson, K. Cao, F. Giustino, and P. Radaelli, $CaBaCo_4O_7$: A ferrimagnetic pyroelectric, Phys. Rev. B **90**, 045129 (2014).

[13] Y. S. Oh, S. Artyukhin, J. J. Yang, V. Zapf, J. W. Kim, D. Vanderbilt, and S.-W. Cheong, Non-hysteretic colossal magnetoelectricity in a collinear antiferromagnet, Nat. Commun. **5**, 3201 (2014).

[14] M. R. Li, D. Walker, M. Retuerto, T. Sarkar, J. Hadermann, P. W. Stephens, M. Croft, A. Ignatov, C. P. Grams, and J. Hemberger, Polar and Magnetic Mn_2FeMO_6 (M = Nb, Ta) with $LiNbO_3$-type Structure: High-Pressure Synthesis, Angew. Chem., Int. Ed. **52**, 8406 (2013).

[15] M.-R. Li, P. W. Stephens, M. Retuerto, T. Sarkar, C. P. Grams, J. Hemberger, M. C. Croft, D. Walker, and M. Greenblatt, Designing polar and magnetic oxides: Zn_2FeTaO_6-in search of multiferroics, J. Am. Chem. Soc. **136**, 8508 (2014).

[16] M. R. Li, M. Retuerto, D. Walker, T. Sarkar, P. W. Stephens, S. Mukherjee, T. S. Dasgupta, J. P. Hodges, M. Croft, and C. P. Grams, Magnetic-structure-stabilized polarization in an above-room-temperature ferrimagnet, Angew. Chem., Int. Ed. **53**, 10774 (2014).

[17] M. R. Li, M. Croft, P. W. Stephens, M. Ye, D. Vanderbilt, M. Retuerto, Z. Deng, C. P. Grams, J. Hemberger, and J. Hadermann, Mn_2FeWO_6: A new Ni_3TeO_6-type polar and magnetic oxide, Adv. Mater. **27**, 2177 (2015).

[18] H. Niu, M. J. Pitcher, A. J. Corkett, S. Ling, P. Mandal, M. Zanella, K. Dawson, P. Stamenov, D. Batuk, A. M. Abakumov, C. L. Bull, R. I. Smith, C. A. Murray, S. J. Day, B. Slater, F. Cora, J. B. Claridge, and M. J. Rosseinsky, Room temperature magnetically ordered polar corundum $GaFeO_3$ displaying magnetoelectric coupling, J. Am. Chem. Soc. **139**, 1520 (2017).

[19] L. Jahnberg, Crystal structure of orthorhombic $CaTa_2O_6$, Acta Chem. Scand. **17**, 2548 (1963).

[20] G. J. Thorogood, M. Avdeev, and B. J. Kennedy, Structural studies of the aeschynite–euxenite transformation in the series $Ln(TiTa)O_6$ Ln = Lanthanide, Solid State Sci. **12**, 1263 (2010).

[21] R. Salmon, H. Baudry, J. Grannec, and G. Le Flem, Sur de nouvelles séries de composés du tungsten +IV de type aeschynite, Rev. Chim. Miner. **11**, 71 (1974).

[22] F. Fauth, I. Peral, C. Popescu, and M. Knapp, The new material science powder diffraction beamline at ALBA synchrotron, Powder Diffr. **28**, S360 (2013).

[23] F. Fauth, R. Boer, F. Gil-Ortiz, C. Popescu, O. Vallcorba, I. Peral, D. Fullà, J. Benach, and J. Juanhuix, The crystallography stations at the Alba synchrotron, Eur. Phys. J. Plus **130**, 160 (2015).

[24] S. Kurtz and T. Perry, A powder technique for the evaluation of nonlinear optical materials, J. Appl. Phys. **39**, 3798 (1968).

[25] K. E. Rieckhoff and W. L. Peticolas, Optical second-harmonic generation in crystalline amino acids, Science **147**, 610 (1965).

[26] K. M. Ok, E. O. Chi, and P. S. Halasyamani, Bulk characterization methods for non-centrosymmetric materials: Second-harmonic generation, piezoelectricity, pyroelectricity, and ferroelectricity, Chem. Soc. Rev. **35**, 710 (2006).

[27] C. De, S. Ghara, and A. Sundaresan, Effect of internal electric field on ferroelectric polarization in multiferroic $TbMnO_3$, Solid State Commun. **205**, 61 (2015).

[28] J. Rodríguez-Carvajal, Recent advances in magnetic structure determination by neutron powder diffraction, Phys. B Condens. Matter **192**, 55 (1993).

[29] S. Ivantchev, E. Kroumova, G. Madariaga, J. Perez-Mato, and M. Aroyo, SUBGROUPGRAPH: A computer program for analysis of group–subgroup relations between space groups, J. Appl. Crystallogr. **33**, 1190 (2000).

[30] V. A. Streltsov and N. Ishizawa, Synchrotron X-ray study of the electron density in $RFeO_3$ (R = Nd, Dy), Acta Crystallogr., Sect. B: Struct. Sci., Cryst. Eng. Mater. **55**, 1 (1999).

[31] A. Kuzmin and J. Purans, Local atomic and electronic structure of tungsten ions in AWO_4 crystals of scheelite and wolframite types, Radiat. Meas. **33**, 583 (2001).

[32] J. Perez-Mato, S. Gallego, E. Tasci, L. Elcoro, G. de la Flor, and M. Aroyo, Symmetry-based computational tools for magnetic crystallography, Annu. Rev. Mater. Res. **45**, 217 (2015).

[33] B. J. Campbell, H. T. Stokes, D. E. Tanner, and D. M. Hatch, ISODISPLACE: A web-based tool for exploring structural distortions, J. Appl. Crystallogr. **39**, 607 (2006).

[34] N. V. Belov, N. N. Nerova, and T. S. Smirnova, Shubnikov groups, Sov. Phys. Crystallogr. **2**, 311 (1957).

[35] We have used the program CRYSCALCON distributed within the FULLPROF suite for calculating the expected ionic polarization assuming formal charges and the experimental structural data.

[36] J. Shieh, J. Yeh, Y. Shu, and J. Yen, Hysteresis behaviors of barium titanate single crystals based on the operation of multiple 90° switching systems, Mater. Sci. Eng.: B **161**, 50 (2009).

[37] See Supplemental Material at http://link.aps.org/supplemental/10.1103/PhysRevB.95.224416 for a detailed structural analysis on $R\mathrm{FeWO}_6$(R = Eu, Tb, and Y).